

Extended X-ray emission from the classic nova DQ Her - On the possible presence of a magnetized jet

J.A. Toalá¹★, M.A. Guerrero², E. Santamaría³, G. Ramos-Larios³ and L. Sabin⁴

¹*Instituto de Radioastronomía y Astrofísica (IRyA), UNAM Campus Morelia, Apartado postal 3-72, 58090 Morelia, Michoacan, Mexico*

²*Instituto de Astrofísica de Andalucía (IAA-CSIC), Glorieta de la Astronomía S/N, 18008 Granada, Spain*

³*Instituto de Astronomía y Meteorología, Universidad de Guadalajara, Av. Vallarta 2602, Arcos Vallarta, 44130 Guadalajara, Mexico*

⁴*Instituto de Astronomía, Universidad Nacional Autónoma de México, Apdo. Postal 877, 22800 Ensenada, B.C., Mexico*

9 April 2024

ABSTRACT

We present an analysis of archival *Chandra* and *XMM-Newton* observations of the magnetically-active cataclysmic variable DQ Her and the shell around it ejected in a nova event in 1934. A careful revision of the *Chandra* observations confirms previous claims on the presence of extended X-ray emission around DQ Her and reveals that it actually corresponds to a bipolar jet-like structure extending $\approx 32''$ along a direction from NE to SW. Therefore, this X-ray emission extends beyond the optical nova shell and is perpendicular to its major axis. The *XMM-Newton* observations confirm the presence of the extended X-ray emission detected by *Chandra*, suggesting the additional presence of a diffuse X-ray emission from a hot bubble filling the nova shell. This hot bubble was very likely produced by the explosion that created the nebular shell detected in optical images. The bipolar feature can be modelled by the combination of an optically thin plasma emission component with temperature $T \approx 2 \times 10^6$ K and a power law component with a photon index of $\Gamma = 1.1 \pm 0.9$. Its X-ray luminosity in the 0.3–5 keV energy range is $L_X = (2.1 \pm 1.3) \times 10^{29}$ erg s^{−1}, for an electron density $n_e \approx 2$ cm^{−3} and a mass $m_X \approx 3 \times 10^{-6} M_\odot$. We suggest that the X-ray bipolar structure in DQ Her is a jet and interpret its non-thermal X-ray emission in terms of a magnetized jet.

Key words: stars: evolution — stars: dwarf novae — (stars:) novae, cataclysmic variables — X-rays: individual: DQ Her

1 INTRODUCTION

The detection of extended X-ray emission from classical novae (CNe) has proven to be rare. Thorough archival studies searching for diffuse X-ray emission from nova shells have been presented in the past (e.g., [Orio et al. 2001](#); [Balman 2006](#)), but there is only a handful number of novae with reported extended X-ray emission.

The first detection of extended X-ray emission in a CN was obtained for GK Per using *ROSAT* PSPC observations ([Balman, & Ögelman 1999](#)). Subsequent observations of GK Per by the *Chandra* X-ray observatory ([Balman 2005](#)) demonstrated that its extended X-ray emission can be described by a non-equilibrium thermal plasma component with additional synchrotron emission. With a total energy $\sim 10^{-7}$ times that of a classic supernova explosions ($\sim 10^{51}$ erg s^{−1}), the diffuse X-ray emission from GK Per is a scaled down version of those events. More recent *Chandra* observations showed that the X-ray brightness of GK Per declines with time as a result of its expansion ([Takei et al. 2015](#)), implying that the diffuse X-ray emission from CNe is short-lived. The dramatic morphologi-

cal and spectral variations of its X-ray emission revealed by *Sukaku* observations probe the interactions of this nova remnant through its complex circumstellar medium ([Yuasa et al. 2016](#)).

Extended X-ray emission has also been reported in *Chandra* observations of RR Pic ([Balman, & Küpcü-Yoldaş 2004](#)), although the marginal detection (~ 60 photons) makes difficult an assessment of the spatial correlation of the extended X-ray emission with the optical nova shell (see figure 1 in [Balman 2006](#)). Marginal detections of extended X-ray emission have been claimed for the recurrent nova T Pyx ([Balman 2014](#)) and the cataclysmic variable (CV) DK Lac ([Takei et al. 2013](#)), but the former has been questioned ([Montez et al. 2012](#)). Finally, an extended $1'2''$ jet-like feature in the soft (0.3–0.8 keV) energy band has been reported in *Chandra* observations of the recurrent nova RS Oph ([Luna et al. 2009](#)). The orientation of this extended X-ray emission is consistent with the radio and IR emission from the ring of synchrotron-emitting plasma associated with the most recent blast wave ([Chesneau et al. 2007](#)).

In this work we focus on the extended X-ray emission from DQ Her, a slow nova from a CV system that experienced an outburst on December 1934 and ejected a nova shell with a present angular size of $32'' \times 24''$ ([Santamaría et al. 2020](#)). This classical nova was

★ E-mail: j.toala@irya.unam.mx

not initially detected by *Einstein* (Cordova et al. 1981), but Silber et al. (1996) reported its detection in *ROSAT* Position Sensitive Proportional Counters (PSPC) observations with an X-ray luminosity in the 0.1–2.0 keV energy range of $4 \times 10^{30} \text{ erg s}^{-1}$. The low number of photons detected in these observations precluded at that time a detailed characterization of the X-ray properties from DQ Her. Higher quality *Chandra* Advanced CCD Imaging Spectrometer (ACIS)-S observations were used by Mukai et al. (2003) to study the spectral properties and time variation of the X-ray-emitting, magnetically-active progenitor star of DQ Her (e.g., Walker 1956). Mukai et al. (2003) found that the best-fit model to the X-ray spectrum of the progenitor star of DQ Her is composed by an optically-thin plasma emission model plus a power-law, the latter component in line with the magnetic field of DQ Her. Furthermore, their analysis of radial profiles of the X-ray emission hinted at the presence of extended X-ray emission with energies below 0.8 keV at distances up to $\sim 10''$ from DQ Her that they associated with individual clumps in the nova shell.

We present here a joint analysis of archival *XMM-Newton* European Photon Imaging Camera (EPIC) observations and revisit the *Chandra* ACIS-S observations of DQ Her. The combination of both archival data confirms that the extended X-ray emission from DQ Her is indeed real and originates from emission filling the nova shell and a bipolar (jet-like) feature. This paper is organised as follows. In Section 2 we describe the observations analysed here. The results of the imaging and spectral analyses are presented in Section 3 and 4, respectively. A discussion of our results is presented in Section 5 and a summary in Section 6.

2 OBSERVATIONS AND DATA PREPARATION

2.1 Chandra Observations

DQ Her was observed by the *Chandra* X-ray Observatory with a total exposure time of 70 ks split into two observations performed on 2001 July 26 and 29. The back-illuminated S3 CCD on the ACIS-S was used for these observations (Obs. ID. 1899 and 2503, PI: K. Mukai). The ACIS-S data were reprocessed with the *Chandra* Interactive Analysis of Observations (CIAO) software (version 4.11; Fruscione et al. 2006). After combining the data and excising high-background and dead periods of time, the net exposure time was 68 ks. X-ray images of DQ Her obtained after combining the two data sets are presented in Figure 1.

The processed event *Chandra* image of DQ Her in the 0.3–5.0 keV energy range (Fig. 1 - top) undoubtedly shows that the central star is a point-source of X-ray emission. To unveil the true extension of the diffuse X-ray emission in DQ Her, we created a smoothed image in the 0.3–5.0 keV energy range using the CIAO task *csmooth*. The smoothing process was performed using a Gaussian kernel and a fast-Fourier transform (FFT) convolution method. Regions in the event file above 3σ -confidence levels remained unsmoothed, preventing the emission from the central star to be highly smoothed. The resultant image is shown in the bottom panel of Figure 1, where a highly elongated extended emission along the NE-SW direction is clearly shown. Alternatively, we used the suite MARX 5.5.0 (Davis et al. 2012) to model the *Chandra* point spread function (PSF) of a point-source with the spectral properties of the central star of DQ Her (as described by Mukai et al. 2003, but see also section 4.1 below). The comparison of this synthetic X-ray point-source with the image of DQ Her confirms the presence and extent of this diffuse emission.

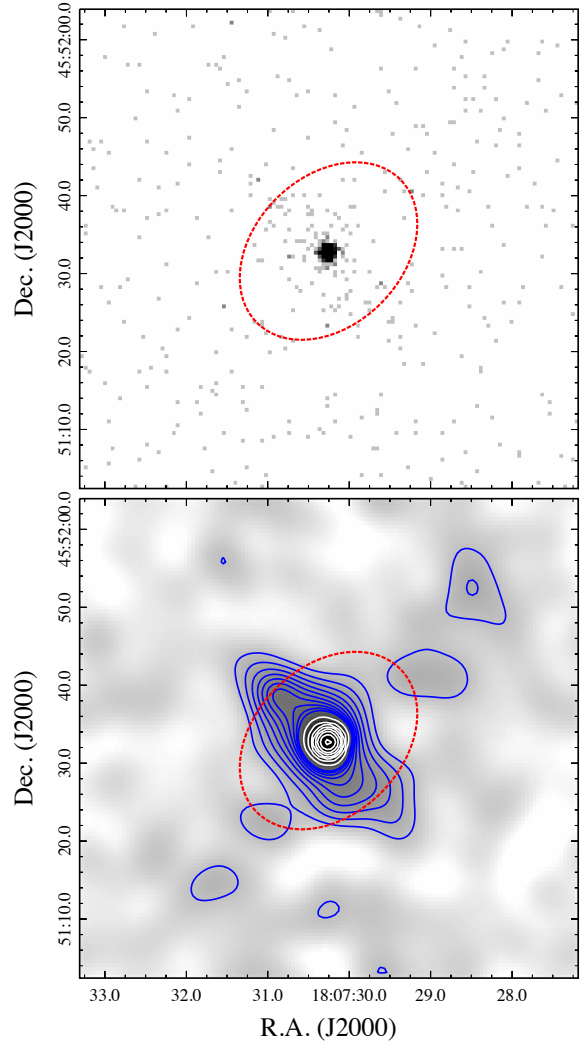


Figure 1. *Chandra* ACIS-S images of DQ Her. Top panel: An image of the event file using the natural $0''.5$ in size ACIS-S pixel. Bottom: Adaptively smoothed image of the extended X-ray emission in DQ Her detected by *Chandra*. Both images were obtained in the 0.3–5.0 keV energy range. The dashed ellipse shows the extent of the optical nebula as presented in Figure 3.

The *Chandra* spectra of the central star and that of the extended emission were extracted separately from each ACIS observations using the CIAO task *specextract*, which produces the corresponding calibration matrices. The spectra and calibration matrices from different data sets were subsequently merged using the CIAO task *combine_spectra*. The spectrum of the central star of DQ Her was extracted from a circular aperture with radius of $2''$ and that of the extended X-ray emission from an elliptical aperture with semi-minor and major axes $10''$ and $18''$ encompassing the emission detected in the bottom panel of Figure 1. The emission from the central source was excised from the latter. The background was extracted from a region without contribution from extended emission nor point sources. The net count rates in the 0.3–5.0 keV energy range are $22.6 \text{ counts ks}^{-1}$ for the central star and $1.32 \text{ counts ks}^{-1}$ for the extended emission for total count numbers $\approx 1,500$ and ≈ 90 counts, respectively.

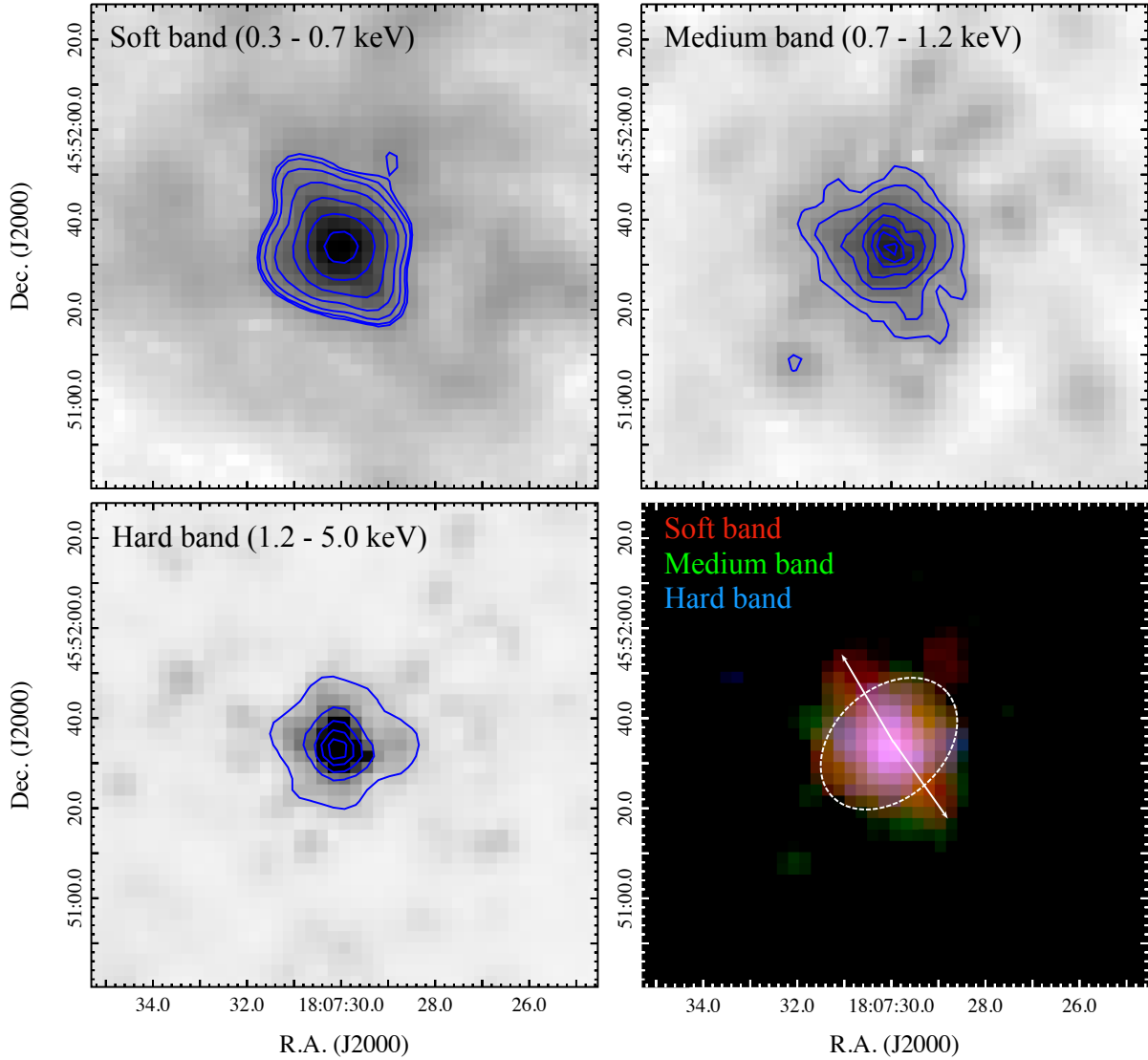


Figure 2. *XMM-Newton* EPIC (pn+MOS1+MOS2) images of DQ Her. The bottom right panel shows a colour-composite image obtained by combining the other three panels. Red, green and blue correspond to the soft, medium and hard bands. The extension of the nebular remnant detected in optical observations (see Fig. 3) is shown with an elliptical dashed-line region. The suggested bipolar structure is shown with arrows.

2.2 *XMM-Newton* Observations

DQ Her was observed by *XMM-Newton* on 2017 April 19 with the three EPIC cameras for a total exposure time of 41.9 ks (PI: H. Worpel; Obs. ID.: 0804111201). The EPIC pn, MOS1 and MOS2 cameras were operated in the Full Frame Mode with the thin optical blocking filter. The individual observing times for the pn, MOS1, MOS2, and pn cameras were 39.0 ks, 40.6 ks, and 40.5 ks, respectively. The *XMM-Newton* data were processed with the Science Analysis Software (sas; version 17.0), using the *epproc* and *emproc* SAS tasks to apply the most recent calibrations available on February 2020. After excising periods of high background, the total useful time of the pn, MOS1 and MOS2 cameras were 15.2 ks, 25.4 ks and 26.2 ks, respectively.

We used the Extended Source Analysis Software (ESAS) tasks to map the distribution of the X-ray-emitting gas in DQ Her. Background-subtracted, exposure-corrected EPIC pn, MOS1, and

MOS2 images were created and merged. EPIC images in the soft 0.3–0.7 keV, medium 0.7–1.2 keV, and hard 1.2–5.0 keV energy bands were created. The individual images and a colour-composite X-ray picture are presented in Figure 2.

Spectra and their corresponding associated calibration matrices were obtained from a circular aperture with radius of $24''$ centered on the central star of DQ Her using the *evselect*, *arfgen* and *rmfgen* sas tasks. Due to the lower spatial resolution of the EPIC cameras compared to that of ACIS-S, the contribution from the central star cannot be properly resolved from that of the extended X-ray emission. Therefore, the EPIC spectra encompass the emission from both the point-source and extended component of DQ Her. The net count rates of the pn, MOS1 and MOS2 cameras are $41.9 \text{ counts ks}^{-1}$, $8.4 \text{ counts ks}^{-1}$, and $11.6 \text{ counts ks}^{-1}$, respectively.

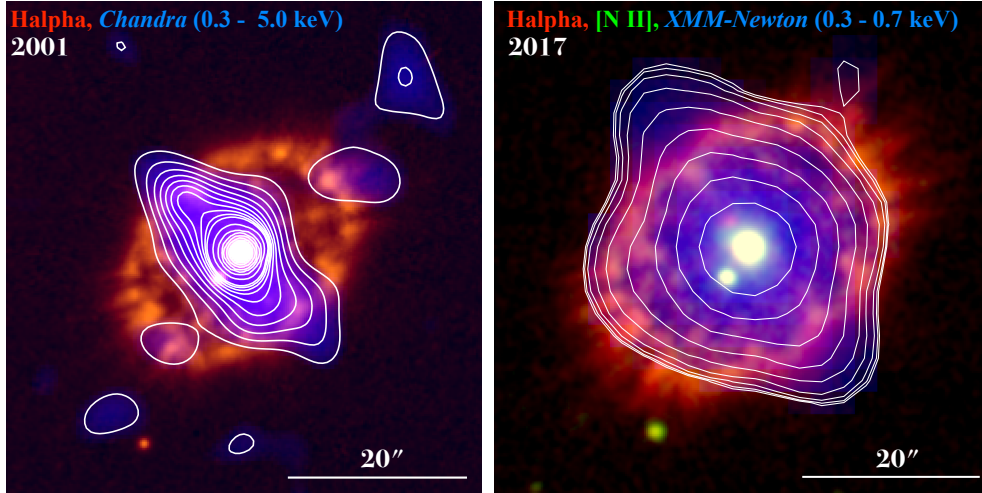


Figure 3. Comparison between the optical emission from DQ Her and the X-ray observations obtained with *Chandra* (left) and *XMM-Newton* (right). The nebular images from 2017 were obtained at the NOT and the corresponding $H\alpha$ 2001 image was obtained by expanding a WHT from 1997 by 6% according to [Santamaría et al. \(2020\)](#) (see Section 3 for details).

3 EXTENDED X-RAY EMISSION FROM DQ HER

The *Chandra* ACIS-S images presented in Figure 1 clearly confirms the presence of extended emission as previously reported by [Mukai et al. \(2003\)](#). More importantly, the X-ray image in the bottom panel of this figure shows that this emission has a bipolar, jet-like shape $\approx 16''$ wide and $\approx 32''$ long in the NE to SW direction ($PA \approx 45^\circ$). The direction of this bipolar feature is orthogonal to the apparent semi-major axis of the nebula. The *Chandra* X-ray image shows that the bipolar feature presents hints of an S-shape, more clearly seen in its SW section.

The *XMM-Newton* EPIC images presented in Figure 2 also show extended X-ray emission. The images in the three X-ray bands present a peak at the location of the central star of DQ Her, as well as extended emission that, depending on the X-ray band, uncover different features. The soft (0.3–0.7 keV) EPIC X-ray image (Fig. 2 top left) is indicative of a bipolar morphology protruding from the central star and extending towards the NE and SW directions, very similar to that of the extended X-ray emission detected in the *Chandra* images. The diffuse emission detected in the medium (0.7–1.2 keV) EPIC X-ray band (Fig. 2 - top right) also extends towards the NE and SW regions, but this component is not spatially coincident with the bipolar features detected in the soft band. Instead, it seems to surround the soft emission. Finally, the spatial distribution of the emission in the hard (1.2–5.0 keV) EPIC X-ray band is more centrally-concentrated than in the other two EPIC bands (see Fig. 2 - bottom left) and is basically consistent with a point-source with some contribution to the extended emission. All these characteristics are illustrated in the colour-composite X-ray picture presented in the bottom right panel of Figure 2.

To further peer into the spatial distribution of the X-ray-emitting material in DQ Her, we show in Figure 3 a comparison between the X-ray and narrowband optical images. As noted by [Santamaría et al. \(2020\)](#), DQ Her has an angular expansion rate sufficiently large ($0''.188 \text{ yr}^{-1}$ along its major axis) to result in a noticeable angular expansion within a few years. To produce consistent comparisons between the optical nebular remnant and the X-ray images, optical images obtained at similar epochs than those of the X-ray images have to be used. For comparison with the *Chan-*

dra images, the closest contemporary available image of DQ Her is an $H\alpha$ image taken at the William Herschel Telescope (WHT, La Palma, Spain) on 1997 October 25, i.e., about 4 years before the X-ray observation. An expansion factor of 6% was applied to this optical image, following the expansion rate reported by [Santamaría et al. \(2020\)](#), to produce a synthetic 2001 $H\alpha$ image suitable for comparison with the *Chandra* X-ray image (Fig. 3 - left). For comparison with the *XMM-Newton* images, we used $H\alpha$ and [N II] images obtained at the Nordic Optical Telescope (NOT, La Palma, Spain) on 2017 May 27, just about one month after the X-ray observation (Fig. 3 - right). The inspection of the pictures in Figure 3 clearly reveals that the bipolar jet-like feature extends beyond the optical nebula and is oriented along its minor axis.

4 SPECTRAL ANALYSIS

The superb angular resolution of the *Chandra* ACIS camera has allowed us to extract individual spectra for the point source and extended X-ray emission from DQ Her (Fig. 4-top left and right, respectively). These ACIS spectra reveal remarkable spectral differences between the central and the diffuse emission, as illustrated in the bottom-left panel of Figure 4, regardless of the lower quality of the spectrum of the diffuse component. As shown by [Mukai et al. \(2003\)](#), the spectrum of the star peaks between 0.8–1.0 keV, with some contribution to the soft energy range below 0.7 keV. The spectrum then declines for energies above 1.0 keV showing the contribution from some spectral line very likely the Si XIII at 1.8 keV. On the other hand, the spectrum of the extended emission peaks at softer energies, $\lesssim 0.6$ keV, declining towards higher energies, with hints of the presence of spectral lines at 0.9 keV and 1.4 keV. The former could be attributed to the O VII triplet at 0.58 keV, the Fe complex at ≈ 0.8 keV, and the Ne IX lines at 0.9 keV, and the latter to Mg XI at 1.4 keV.

In the following we present the details of the spectral analysis of the *Chandra* ACIS-S and *XMM-Newton* EPIC spectra of DQ Her. The parameters of the best-fit models for the different spectra as well as their significance are listed in Figure 4 are listed in Table 1.

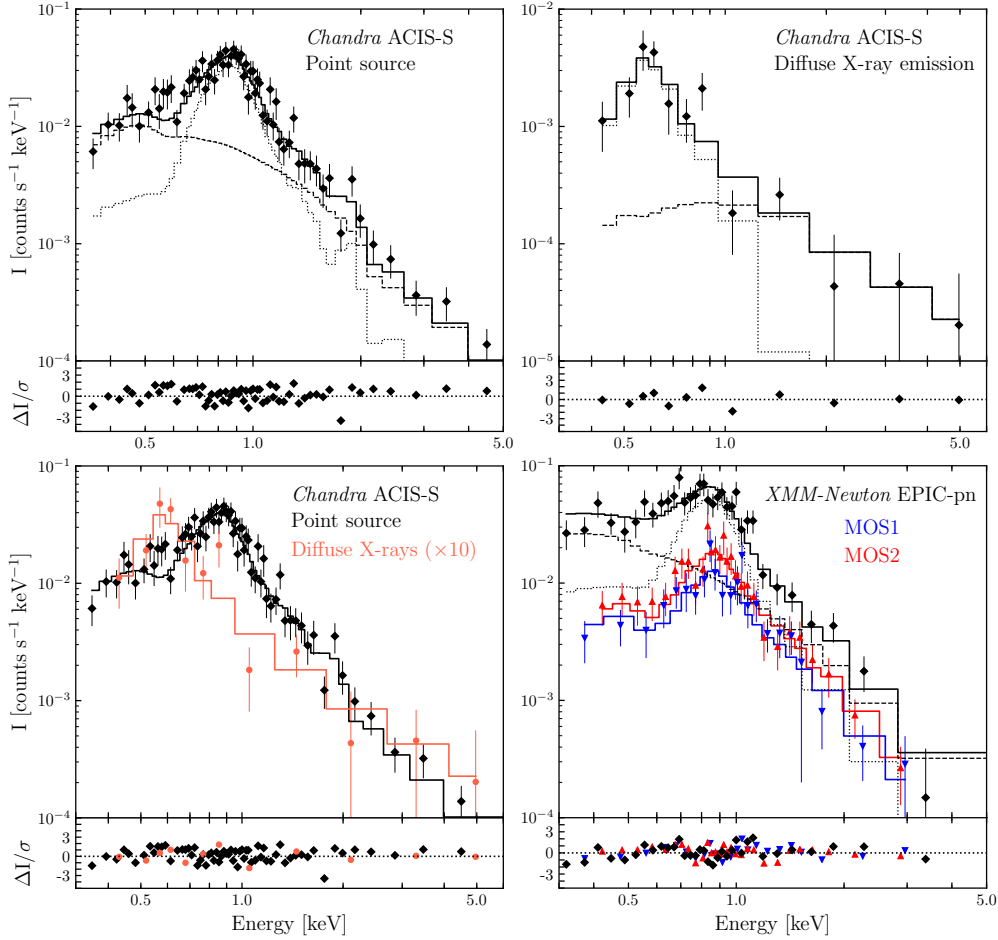


Figure 4. Background-subtracted spectra of DQ Her. The top panels show the *Chandra* ACIS spectra of the point-source (left) and diffuse emission (right). The two spectra are shown together in the bottom-left panel, where the emission from the diffuse component has been scaled for an easy comparison. The bottom-right panel presents the *XMM-Newton* EPIC spectra of DQ Her, with different symbols and colours for the spectra extracted from different EPIC cameras. In all panels the solid lines represent the best-fit model to the data, while the dotted and dashed lines show the contribution of *aptec* and non-thermal power-law components, respectively.

4.1 X-rays from DQ Her

Following Mukai et al. (2003) we fitted a two-component model to the *Chandra* ACIS-S spectra of the central star of DQ Her consisting of an optically-thin *aptec* emission model and a power-law component. The former component can be attributed to a hot plasma and the latter to non-thermal synchrotron emission. Our best fit model, which is presented in the left panel of Figure 4 in comparison with the ACIS-S spectrum, has parameters consistent with those obtained by Mukai et al. (2003) (see Table 1). The non-thermal emission with a power-law index of $\Gamma = 2.45$ dominates in the soft energy range below 0.7 keV and above 1.0 keV, with a contribution $\approx 43\%$ to the total intrinsic flux. The intrinsic flux of DQ Her is found to be $F_X = (9.4 \pm 1.2) \times 10^{-14} \text{ erg s}^{-1} \text{ cm}^{-2}$, implying a luminosity $L_X = (2.8 \pm 0.4) \times 10^{30} \text{ erg s}^{-1}$ at a distance of $501 \pm 6 \text{ pc}$ (Schaefer 2018).

4.2 Extended X-ray emission

The spectrum of the extended bipolar X-ray emission detected in the *Chandra* ACIS-S observations was initially fitted by a single

optically thin *aptec* emission model, but resulted in a poor quality fit with $\chi^2/\text{DoF}=1.60$. A power-law model results in an even worse fit ($\chi^2/\text{DoF}>2.4$), whereas a two-temperature plasma emission model does not improve the fit ($\chi^2/\text{DoF}=1.60$), as it is not able to appropriately fit the spectrum for energies above 2 keV. The best-fit model is achieved by using a similar model as that for the central star, that is, a plasma emission model plus a non-thermal power-law. This best-fit, whose parameters are listed in Table 1, is shown in the middle panel of Figure 4 in comparison with the ACIS-S spectrum. This panel shows that the *aptec* component dominates the emission for energies below 1.0 keV and the power-law component for greater energies. Indeed, the non-thermal component contributes to 40% of the total unabsorbed flux for the 0.3–5.0 keV energy range, but the optically-thin plasma component contributes to 75% of the flux for energies between 0.3 and 1 keV. The luminosity of the extended bipolar emission detected in *Chandra* is $L_{X,\text{diff}} = (2.1 \pm 1.3) \times 10^{29} \text{ erg s}^{-1}$.

To estimate an electron density for the extended X-ray emission we used the definition of the normalization parameter (see Table 1) adopting an ellipsoidal morphology with semi-axes of $8''$, $8''$ and $16''$. The electron density of the bipolar emission is estimated to be $n_e \approx 2 \text{ cm}^{-3}$, which corresponds to a mass of the X-ray-emitting

Table 1. Details of the spectral modelling of the X-ray observations of DQ Her.

	Instrument	N_{H} (10^{20} cm^{-2})	kT (keV)	A_1^b (10^{-5} cm^{-5})	Γ	A_2^b (10^{-5} cm^{-5})	f_X^c (cgs)	F_X^c (cgs)	F_2/F_X^d	χ^2/DoF
DQ Her	ACIS-S	3.4 ± 2.0	$0.77^{+0.05}_{-0.05}$	1.33	$2.45^{+0.50}_{-0.40}$	1.05	8.00 ± 1.10	9.40 ± 1.20	0.43	1.12
Extended	ACIS-S	1.8 ± 0.2	$0.18^{+0.05}_{-0.07}$	0.26	$1.10^{+0.09}_{-0.09}$	0.04	0.64 ± 0.41	0.70 ± 0.47	0.40	1.16
DQ Her+Extended	EPIC-pn	3.4	$0.78^{+0.06}_{-0.07}$	1.15	$2.34^{+0.25}_{-0.21}$	1.20	7.60 ± 1.10	8.90 ± 1.00	0.60	1.08
DQ Her+Extended	EPIC(pn+MOS) ^a	3.4	$0.77^{+0.04}_{-0.05}$	1.20	$2.37^{+0.20}_{-0.20}$	1.20	7.60 ± 1.10	8.90 ± 0.90	0.60	0.90

^aJoint model fit of the EPIC pn, MOS1 and MOS2 spectra.^bThe normalization parameter is defined as $A \approx 10^{-14} \int n_e^2 dV / 4\pi d^2$, where n_e and d are the electron number density and the distance, respectively.^cThe fluxes are computed for the 0.3–5 keV energy range and are presented in $10^{-14} \text{ erg s}^{-1} \text{ cm}^{-2}$ units.^dThe F_2/F_X ratio represents the contribution from the power-law component to the total flux.

material $\approx 3 \times 10^{-6} M_{\odot}$, well below the typical mass ejecta of nova events (e.g., Gehrz et al. 1998; Della Valle & Izzo 2020) and the ionised mass of DQ Her ($2.3 \times 10^{-4} M_{\odot}$; Santamaría et al. 2020).

4.3 The *XMM-Newton* Spectra

Due to the large PSF of the EPIC cameras it is not possible to extract independent spectra for the central star and extended X-ray emission of DQ Her. The three EPIC spectra are shown in the right panel of Figure 4. Similarly to the *Chandra* ACIS spectrum, the *XMM-Newton* EPIC spectra of DQ Her show a main peak for energies around 0.8–1.0 keV with a secondary contribution for energies below 0.7 keV. In addition, these spectra show some contribution from the N VI triplet at 0.43 keV that is not detected in the *Chandra* spectrum due to its lower sensitivity at softer energies.

We first modelled the EPIC-pn spectrum of DQ Her because of its larger count rate than that of the MOS cameras (see Section 2). For simplicity, we fixed the column density value to that obtained to the best-fit model to the ACIS-S data ($N_{\mathrm{H}} = 3.4 \times 10^{20} \text{ cm}^{-2}$) and adopted a similar model consisting of an *apec* plasma emission model for hot gas and a power-law component for non-thermal emission. The best-fit model is consistent with that obtained for the *Chandra* ACIS-S spectrum of the central star of DQ Her (see Table 1). The total luminosity in this model is $L_X = (2.7 \pm 0.3) \times 10^{30} \text{ erg s}^{-1}$, with the power-law component contributing 60% to the total intrinsic flux. Models simultaneously fitting the three EPIC spectra resulted in very similar best-fit parameters (Table 1).

5 DISCUSSION

The spatial and spectral analyses of the *Chandra* and *XMM-Newton* observations of DQ Her presented in Sections 3 and 4 reveal the presence of diffuse X-ray emission with spectral properties differing from those of the central star. Owing to its better angular resolution, $\sim 1''$ at $\leq 1 \text{ keV}$, *Chandra* resolves more clearly the morphology of this emission, which is found to be elongated, extending $\approx 32''$ along the NE-SW direction at $\text{PA} \approx 45^\circ$ (Fig 1 and Fig. 3 - left) with a subtle S-shape. Contrary to Mukai et al. (2003)'s interpretation, this emission is not associated with any specific clump in the nebular remnant, but it extends beyond the optical nova shell along its minor axis.

This morphology is confirmed in the *XMM-Newton* images presented in Figures 2 and 3 right panel, although at a coarse angular resolution ($\sim 6''$ at $\leq 1 \text{ keV}$). The misalignment of the arrows marking the tips of the elongated structure in Figure 3 bottom right panel is indeed consistent with its S-shape in the *Chandra* images.

In addition, the *XMM-Newton* EPIC image in the soft band is suggestive of extended X-ray emission filling the nova shell around DQ Her.

The extended emission in the soft *XMM-Newton* image can be attributed to thermal emission from hot plasma produced by the nova explosion, an adiabatically-shocked hot bubble homologous to supernova explosions. This hot bubble would be spatially coincident with the nebular remnant with no contribution to the bipolar structure detected in X-rays. On the other hand, the origin of the bipolar structure is intriguing. It cannot be attributed to hot gas escaping the nova shell, because its non-thermal component is not expected from shock-heated plasma inside a hot bubble and because it projects along the minor axis of the nova shell whilst the shell is disrupted along its major axis at $\text{PA} = -45^\circ$ (Vaytet et al. 2007).

The production of the bipolar X-ray emission in DQ Her could be argued to be at the origin of the nova explosion. Three-dimensional numerical simulations tailored to similar events, such as outbursts in symbiotic stars (see, e.g., Walder et al. 2008; Orlando et al. 2017), might help interpreting the bipolar X-ray feature in DQ Her. In particular, the simulations presented in Orlando et al. (2017) to model the X-ray emission from the symbiotic star V745 Sco only 17 days after its outburst are able to produce bipolar ejections of X-ray-emitting gas. This X-ray emission arises from a non-isotropic blast wave produced instantaneously at the nova event. Its emission would then be thermal, with physical conditions at early times similar to those of the thermal component of the jet-like feature of DQ Her. However, the non-thermal emission and continuous collimation of the jet in DQ Her, $\sim 80 \text{ yr}$ after the nova event (Santamaría et al. 2020), make these models unsuitable for the case of DQ Her.

It is interesting to note that the CV at the center of DQ Her belongs to the class of magnetically active intermediate polars (IP) exhibiting strong magnetic fields of the order of 1–10 MG (see Barrett et al. 2017, and references therein), which results in the presence of a truncated accretion disk. Indeed Mukai et al. (2003) suggested that the X-ray emission from DQ Her is produced by scattered X-ray photons due to the presence of an accretion disk wind making it an unusual IP system. Furthermore, spectral mapping of DQ Her has revealed that the material in the disk is spiraling-in (Saito et al. 2010). Thus, we suggest that the elongated structure of DQ Her could be interpreted as a magnetized jet produced by *hoop stress* at the inner regions of the accretion disk as it is *threaded* by the vertical magnetic field (Livio 1997). In this scenario, which has been proven feasible in stellar systems, such as the case of the proto-stellar object HH80 (Carrasco-González et al. 2010), the jet would be continuously fed by material falling into the accretion disk and then ejected by the hoop stress. The non-thermal X-ray emission

from the bipolar feature in DQ Her seems to support this scenario. Non-thermal radio emission would lend additional support, as typically found in jets of symbiotic stars (e.g., CH Cyg; Karovska et al. 2010). However, an inspection of Jansky Very Large Array (JVLA) observations of DQ Her discloses the lack of radio emission from either the central source or an extended component (see Barrett et al. 2017). We note that the synchrotron radiation from relativistic electrons close to the accreting white dwarf in CVs (Chanmugam & Dulk 1982) has been found to be highly variable, as it is the case of the central source of DQ Her (Pavelin et al. 1994).

The disk+jet phenomenon is found in a variety of astrophysical systems, from protostellar and young stellar objects (Carrasco-González et al. 2010, 2012), evolved low-mass stars (Sahai et al. 1998), and massive X-ray binaries (van Kerkwijk et al. 1992) to AGNs (Alonso-Herrero et al. 2018). White dwarfs can act as the compact object for jet collimation, and indeed disk+jet systems have been found in symbiotic stars in which a white dwarf accretes material from a main sequence or red giant companion, for example, the well-studied R Aqr (Ramstedt et al. 2018; Schmid et al. 2018; Melnikov et al. 2018) or MCW 560 (Stute & Sahai 2009). On the other hand, the conspicuous absence of jets in CVs has been explained in terms of the particular physical conditions in these systems (Soker & Lasota 2004), although recent observational and theoretical results have found some evidence for transient jets (Coppejans & Knigge 2020).

As for nova shells, Shara et al. (2012) suggested that an elongated structure towards the NE region of GK Per was a jet, but Harvey et al. (2016) demonstrated that it is not dynamically related and it has a low velocity. This leaves us only with the claims of jet-like structures in RS Oph and M31N 2008-12a, two recurrent novae. The presence of a jet in RS Oph is suggested by a jet-like morphological feature with an extent $\sim 1''$ discovered in *Chandra* X-ray observations (Luna et al. 2009). Meanwhile, the presence of a jet in M31N 2008-12a is supported by high-velocity $\sim 4600 \pm 600$ km s⁻¹ features detected in *Hubble Space Telescope* (HST) Space Telescope Imaging Spectrograph (STIS) spectra (Darnley et al. 2017), which are interpreted as an ejecta expanding in the direction close to the line of sight (see also Darnley et al. 2016, and references therein). Since the jet in RS Oph has an X-ray extent close to *Chandra*'s PSF and that of M31N 2008-12a is only detected kinematically, DQ Her presents the best case for the detection of a resolved X-ray jet in a nova shell. We remark that, unlike RS Oph and M31N 2008-12a, which are recurrent novae, the nova shell of DQ Her is associated with a CV.

6 SUMMARY

We have presented the analysis of archival *Chandra* ACIS-S and *XMM-Newton* EPIC observations of the CV DQ Her. Our analysis has shown the presence of diffuse emission with a bipolar, jet-like morphology that extends up to distances $16''$ from the progenitor star along the minor axis of the nova shell, thus protruding away from the nova shell.

We have also shown that the *XMM-Newton* soft band image traces emission both from the jet and from a hot bubble filling the nebula around DQ Her. The latter has been formed as a result of an adiabatically-shocked blast wave very similar to supernova explosions.

The spectra of the extended X-ray emission is notably different to that of DQ Her, exhibiting the presence of emission lines from the O VII triplet at 0.58 keV, the Ne and Fe complex at 0.9 keV, and

Mg XI at 1.4 keV. The bipolar structure has a plasma temperature of 2×10^6 K with an X-ray luminosity in the 0.3–5.0 keV energy range of $L_{X,\text{diff}} = (2.1 \pm 1.3) \times 10^{29}$ erg s⁻¹. Its electron density and estimated mass are $n_e \approx 2$ cm⁻³ and $m_X \approx 3 \times 10^{-6}$ M_⊙, respectively.

We propose that the bipolar structure detected with *Chandra* and *XMM-Newton* is a jet. Its non-thermal emission component strongly supports that it is a magnetized jet, arising as the result of the *hoop stress* mechanism observed in other stellar systems. Under this scenario the jet would be continuously fed by material that falls into the accretion disk and is then ejected by the hoop stress. The S-shape morphology of the jet could then be associated with the precession of the accreting disk at the core of DQ Her or with erratic jet wobbling.

The capabilities of the up-coming *Athena* X-ray satellite will be able to resolve the morphological and spectral components in DQ Her and will help bringing light into the scenario proposed by the present work.

ACKNOWLEDGEMENTS

We would like to thank the referee for prompt revision and useful comments that helped improve the presentation of our results. We also thank C. Carrasco-González for analysing the available JVLA observations of DQ Her. JAT, MAG and GR-L are supported by the UNAM Dirección General de Asuntos del Personal Académico (DGAPA) through the Programa de Apoyo a Proyectos de Investigación e Innovación Tecnológica (PAPIIT) projects IA100318 and IA100720. MAG acknowledges support from grant PGC2018-102184-B-I00, co-funded with FEDER funds. GR-L acknowledge support from Consejo Nacional de Ciencia y Tecnología (CONACyT) and Programa para el Desarrollo Profesional (PRODEP) Mexico. LS acknowledge support from UNAM DGAPA PAPIIT project IN101819. This work has made extensive use of the NASA's Astrophysics Data System. ES thanks CONACyT (Mexico) for a research studentship. This work was based on observations obtained with *XMM-Newton*, an ESA science mission with instruments and contributions directly funded by ESA Member States and NASA. The scientific results reported in this article are based on observations made by the *Chandra* X-ray Observatory and published previously in cited articles.

REFERENCES

- Alonso-Herrero, A., Pereira-Santaella, M., García-Burillo, S., et al. 2018, *ApJ*, 859, 144
- Balman, Ş., & Küpcü-Yoldaş, A. 2004, IAU Colloq. 190: Magnetic Cataclysmic Variables, 172
- Balman, Ş. 2006, *Advances in Space Research*, 38, 2840
- Balman, Ş. 2005, *ApJ*, 627, 933
- Balman, Ş. 2014, *A&A*, 572, 114
- Balman, Ş., & Ögelman, H. B. 1999, *ApJ*, 518, L111
- Barrett, P. E., Dieck, C., Beasley, A. J., et al. 2017, *AJ*, 154, 252
- Carrasco-González, C., Galván-Madrid, R., Anglada, G., et al. 2012, *ApJ*, 752, L29
- Carrasco-González, C., Rodríguez, L. F., Anglada, G., et al. 2010, *Science*, 330, 1209
- Chanmugam, G., & Dulk, G. A. 1982, *ApJ*, 255, L107
- Chesneau, O., Nardetto, N., Millour, F., et al. 2007, *A&A*, 464, 119
- Coppejans, D., & Knigge, C. 2020, arXiv e-prints, arXiv:2003.05953
- Cordova, F. A., Mason, K. O., & Nelson, J. E. 1981, *ApJ*, 245, 609
- Darnley, M. J., Hounsell, R., Godon, P., et al. 2017, *ApJ*, 847, 35

- Darnley, M. J., Henze, M., Bode, M. F., et al. 2016, *ApJ*, 833, 149
- Davis, J. E., Bautz, M. W., Dewey, D., et al. 2012, *Proc. SPIE*, 84431A
- Della Valle, M., & Izzo, L. 2020, arXiv e-prints, arXiv:2004.06540
- Fruscione, A., McDowell, J. C., Allen, G. E., et al. 2006, *Proc. SPIE*, 62701V
- Gehrz, R. D., Truran, J. W., Williams, R. E., et al. 1998, *PASP*, 110, 3
- Harvey, E., Redman, M. P., Boumis, P., et al. 2016, *A&A*, 595, A64
- Karovska, M., Gaetz, T. J., Carilli, C. L., et al. 2010, *ApJ*, 710, L132
- Livio, M. 1997, *IAU Colloq. 163: Accretion Phenomena and Related Outflows*, 845
- Luna, G. J. M., Montez, R., Sokoloski, J. L., et al. 2009, *ApJ*, 707, 1168
- Melnikov, S., Stute, M., & Eisloffel, J. 2018, *A&A*, 612, A77
- Montez, R., Sokoloski, J. L., & Nelson, T. 2012, *The Astronomer’s Telegram* 4097, 1
- Mukai, K., Still, M., & Ringwald, F. A. 2003, *ApJ*, 594, 428
- Orio, M., Covington, J., & Ögelman, H. 2001, *A&A*, 373, 542
- Orlando, S., Drake, J. J., & Miceli, M. 2017, *MNRAS*, 464, 5003
- Pavelin, P. E., Spencer, R. E., & Davis, R. J. 1994, *MNRAS*, 269, 779
- Ramstedt, S., Mohamed, S., Olander, T., et al. 2018, *A&A*, 616, A61
- Sahai, R., Hines, D. C., Kastner, J. H., et al. 1998, *ApJ*, 492, L163
- Saito, R. K., Baptista, R., Horne, K., et al. 2010, *AJ*, 139, 2542
- Santamaría, E., Guerrero, M. A., Ramos-Larios, G., et al. 2020, *ApJ*, 892, 60
- Schaefer, B. E. 2018, *MNRAS*, 481, 3033
- Schmid, H. M., Bazzon, A., Roelfsema, R., et al. 2018, *A&A*, 619, A9
- Shara, M. M., Zurek, D., De Marco, O., et al. 2012, *AJ*, 143, 143
- Silber, A. D., Anderson, S. F., Margon, B., et al. 1996, *ApJ*, 462, 428
- Soker, N., & Lasota, J.-P. 2004, *A&A*, 422, 1039
- Stute, M., & Sahai, R. 2009, *A&A*, 498, 209
- Takei, D., Drake, J. J., Yamaguchi, H., et al. 2015, *ApJ*, 801, 92
- Takei, D., Sakamoto, T., & Drake, J. J. 2013, *AJ*, 145, 18
- van Kerkwijk, M. H., Charles, P. A., Geballe, T. R., et al. 1992, *Nature*, 355, 703
- Vaytet, N. M. H., O’Brien, T. J., & Rushton, A. P. 2007, *MNRAS*, 380, 175
- Walder, R., Folini, D., & Shore, S. N. 2008, *A&A*, 484, L9
- Walker, M. F. 1956, *ApJ*, 123, 68
- Yuasa, T., Hayashi, T., & Ishida, M. 2016, *MNRAS*, 459, 779